Processing and Application of Ceramics 17 [2] (2023) 113–117
https://doi.org/10.2298/PAC2302113M

Heavily doped high-entropy $A_2B_2O_7$ pyrochlore

Branko Matović[1,2,*], Jelena Maletaškić[1], Vesna Maksimović[1], Jelena Zagorac[1], Aleksa Luković[1], Yu-Ping Zeng[2], Ivana Cvijović-Alagić[1]

[1]*Center of Excellence "CEXTREME LAB", Vinča Institute of Nuclear Sciences - National Institute of the Republic of Serbia, University of Belgrade, Mike Petrovića Alasa 12-14, 11001 Belgrade, Serbia*
[2]*State Key Laboratory of High Performance Ceramics and Superfine Microstructure, Shanghai Institute of Ceramics, Chinese Academy of Sciences, 1295 Ding-xi Road, Shanghai 200050, China*

Received 30 September 2022; Received in revised form 16 January 2023; Received in revised form 9 February 2023; Accepted 23 March 2023

Abstract

A novel class of high-entropy pyrochlore compounds with multiple elements at the A and B site positions ($A_2B_2O_7$) was successfully obtained. Powders with $(La_{1/7}Sm_{1/7}Nd_{1/7}Pr_{1/7}Y_{1/7}Gd_{1/7}Yb_{1/7})_2(Sn_{1/3}Hf_{1/3}Zr_{1/3})_2O_7$ nominal composition were fabricated from pure metal oxides obtained through a reaction of metal nitrates (for site A) and metal chlorides (for site B) with sodium hydroxide during the solid-state displacement reaction (SSDR). The phase evolution was analyzed using XRD method. During the thermal treatment of ten individual metal oxides, the single pyrochlore phase was created. The present study showed that the high-density (98 %TD) ceramics with a hardness of 8.1 GPa was successfully obtained after pressureless sintering at 1650 °C for 4 h. Results of the Raman study and the Rietveld structural refinement showed that sintered high-entropy ceramics is characterized by a single-phase pyrochlore structure, which was investigated in detail.

Keywords: *high-entropy oxide, pyrochlore, phase evolution, XRD, microstructure, hardness*

I. Introduction

Modern structural materials must fulfil the demands of new and innovative technologies. Traditional ceramic materials, such as oxide ceramics, cannot support all these requirements and, as a result, in recent years the development of novel high-entropy materials (HEM) was proposed [1–4]. Pyrochlores represent a large class of oxide compounds, both natural and artificial, with $A_2B_2O_6O'$ general formula related to their space group (Z = 8). In the structure of pyrochlores, sites A and B are usually occupied by 3+ and 4+ cations, respectively, while oxygen can take two different positions (O and O′) [5]. Pyrochlore structure can also be considered as a superstructure derivate of the simpler fluorite structure (AO_2) with the $Fm3m$ space group, where A and B cations are ordered along the <110> atomic plane direction and one-eighth of the oxygen ions are absent. The A, B, O, and O′ ions occupy four crystalline sites 16c, 16d, 48f, and 8b, respectively. The unoccupied site corresponds to the oxygen vacancy, which resides in the tetrahedral interstitial site between the adjacent B-sites, causing the reduction of the coordination number of the B-site from 8 to 6. However, the A-site coordination number, i.e. 8, is unchanged. Therefore, pyrochlores have a diverse range of constituent ions that enable the tailoring of a wide range of compounds with different properties. Namely, a random equiatomic distribution of 5 or more elements in the same crystal lattice can induce a local distortion of the lattice with high configurational entropy, which in turn enables the high stability of such compositionally complex compound as a single phase. It was shown that the high-entropy effect in oxides characterized with a single high-entropy phase leads to the obtainment of better properties compared to the properties of every separate individual constituent metal oxide [6]. Hence, a wide range of distinct properties, such as electrical and ionic conductivity [7], geometrically frustrated magnetism [8], neutron absorption [9], nuclear waste storage capacity [10], thermal conductivity [11], photocatalytic ability [12], and scintillator host behaviour [13], can be controlled by changing the constituent ions.

* Corresponding author: tel: +381 11 3408 224
e-mail: *mato@vinca.rs*

Available research reports show that a wide variety of methods was successfully used for the synthesis of the $A_2B_2O_7$ powders, such as solid-state reaction, molten salt synthesis, hydrothermal process, solvothermal synthesis, sol-gel method and combustion method [14–21].

In terms of the industrial commercialization of the production process, the solid-state method is the most favourable due to its cost-effectiveness and intrinsic simplicity. In addition, a significant number of diverse oxide compounds and their solid solutions can be obtained utilizing this method. Therefore, it can be assumed that this method could be also effectively employed for the synthesis of multicomponent oxides, such as high-entropy pyrochlores. The focus of this study, therefore, was to obtain the high-entropy multicomponent oxide with the $A_2B_2O_7$ pyrochlore structure that contains 7 different cations in the A-site and 3 cations in the B-site position in equiatomic amounts by applying the solid-state reaction method. The phase evolution during the calcination process and the sinterability of the obtained powders, as well as some mechanical properties of the sintered high-entropy multicomponent oxide were investigated.

II. Experimental

2.1. Material synthesis

Pure homemade La_2O_3, Sm_2O_3, Nd_2O_3, Pr_2O_3, Y_2O_3, Gd_2O_3, Yb_2O_3, ZrO_2, HfO_2 and SnO_2 oxides in the powder form were employed as precursors for the high-entropy pyrochlore synthesis. The pure homemade oxides were synthesized using the same synthesis method and were as such used as precursors for the high-entropy pyrochlore preparation instead of the commercial oxides because in this way the influence of different synthesis procedures on the behaviour of oxides, especially on their reactivity, was avoided. Starting reactants for the synthesis of the above-mentioned pure oxides were trivalent lanthanide (La, Sm, Nd, Pr, Y, Gd, Yb) nitrate powders in the hydrated form, tetravalent Zr, Hf, and Sn chloride powders, and sodium hydroxide granules supplied by Merck, USA. Amounts of all starting reactants were calculated according to the nominal composition of each particular oxide.

In general, synthesis reaction took place according to Eq. 1 for trivalent cations and Eq. 2 for tetravalent cations as follows:

$$2\,Me^{III}(NO_3)_3 \cdot 6\,H_2O + 6\,NaOH \longrightarrow Me_2O_3 + \\ + 6\,NaNO_3 + 15\,H_2O \quad (1)$$

$$Me^{IV}Cl_4 + 4\,NaOH \longrightarrow MeO_2 + 4\,NaCl + \\ + 2\,H_2O + O_2 \quad (2)$$

where Me^{III} represents La, Sm, Nd, Pr, Y, Gd, Yb, whilst Me^{IV} denotes Zr, Hf and Sn. Reactions presented in Eq. 1 and Eq. 2 are given in simplified form although these are very complex and multi-stage processes [22].

After the synthesis of pure oxides, the high-entropy pyrochlore was prepared using the conventional solid-state method. The appropriate stoichiometric quantities of synthesized oxide powders were homogenized using a ball milling procedure and then uniaxially pressed under the pressure of 100 MPa in the stainless steel die with 10 mm in diameter. Calcination of the obtained powders was undertaken in the temperature range from 750 to 1500 °C for 120 min. Subsequently, the green compacted cylindrical samples, obtained by uniaxial pressing at 100 MPa, were pressureless sintered at 1650 °C for 4 h with a heating rate of 10 °C/min without additive addition in the air atmosphere. These sintering conditions are commonly used for the densification of oxide ceramics with a high melting point, and, at the same time, these conditions mimic the conditions that are applied in the ceramics industry production processes.

2.2. Materials characterization

All calcined powders, as well as the sintered ceramic pellet, were characterized by X-ray diffraction (XRD) technique using the RIGAKU Ultima IV diffractometer, Rigaku, Japan. Crystal structures of the analysed materials were examined by filtered Cu Kα radiation (1.54178 nm) in the 2θ range from 10° to 90°. Phase analysis was enabled by utilization of the PDXL2 software v.2.0.3.0 [23], with reference to the patterns of the International Centre for Diffraction Data (ICDD) v. 2012. The recorded XRD data were used for the additional Rietveld structural refinement analysis and relevant structural parameters of the powders calcined at different temperatures were determined using the FullProf software.

DXR Raman spectrometer, Thermo Fisher Scientific Inc., USA, equipped with an Ar laser operating at an irradiation wavelength of 532 nm was used for analysis of the sintered high-entropy pyrochlore ceramic material.

Microstructural characterization of the obtained high-entropy pyrochlore ceramics was conducted by field-emission scanning electron microscopy (FE-SEM) and for that purpose a JEOL-5200F scanning electron microanalyser was employed.

The sintered sample density was determined by applying the Archimedes principle in distilled water. Measurements showed excellent reproducibility and the corresponding standard deviation was determined to be ± 0.027 g/cm^3. Since the high-entropy pyrochlore crystallizes in space group 227, the theoretical density of this material was calculated according to the proportional ratio of cations present in the material nominal composition.

The microhardness of the sintered high-entropy ceramics was investigated using the Vickers indentation hardness tester model Micromet 5101, Buehler, Germany, by applying a load of 9807 mN for 15 s. The microhardness values were determined at 12 measuring points for each sample with excellent reproducibility with a standard deviation of ± 0.189 GPa.

III. Results and discussion

The crystal structure of pyrochlores is highly dependent on the A-site cation ($r_{A^{3+}}$) and B-site cation ($r_{B^{4+}}$) radii ratio. It is experimentally confirmed that the pyrochlore-type structure is formed for radii ratio $r_{A^{3+}}/r_{B^{4+}}$ = 1.46–1.78 [5]. The case when one site is occupied by several potential elements is especially interesting since this leads to the formation of a high-entropy pyrochlore structure [24]. In this study, the $r_{A^{3+}}/r_{B^{4+}}$ ratio was 1.5257 since 7 different trivalent metal elements are positioned in the A-site and 3 tetravalent metal elements are positioned in the B-site indicating that the formation of a stable pyrochlore structure is ensured. The successful formation of the single phase material is considered through XRD analysis of the powders that are experimentally obtained during the calcination process. The XRD patterns of the powders calcined at different temperatures for 2 h are presented in Fig. 1.

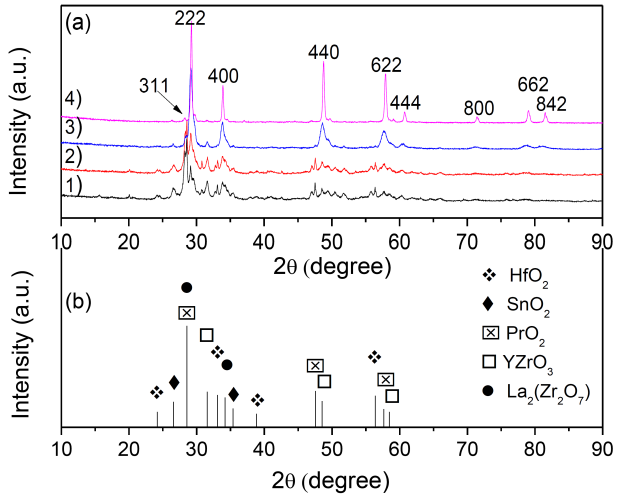

Figure 1. XRD patterns (a) of the calcined pyrochlore powders isothermally treated for 2 h at: 1) 750 °C, 2) 900 °C, 3) 1200 °C and 4) 1500 °C; identification of additional phases (b) present in the calcined powder isothermally treated for 2 h at 750 °C

At the lowest calcination temperature (750 °C), in addition to starting oxides, i.e. HfO_2, SnO_2 and PrO_2, more complex phases, such as $YZrO_3$ and $La_2Zr_2O_7$, were observed. The reaction takes place in the solid state, however, due to the different diffusion of individual cations, the formation of intermediate phases occurs at the beginning of the process. The process intensifies with an increase in temperature till the temperature of 1200 °C is reached and one phase dominates in the final structure. Namely, the X-ray profiles show the phase evolution of many individual oxides to only one phase with disorder-defective fluorite structure during the calcination at 1200 °C. On the presented XRD patterns a considerable broadening of diffraction lines can be observed indicating a low crystallinity and small crystallite size of the obtained material. However, an increase in the heat treatment temperature promotes the crystallization of a compound with a pyrochlore structure. XRD

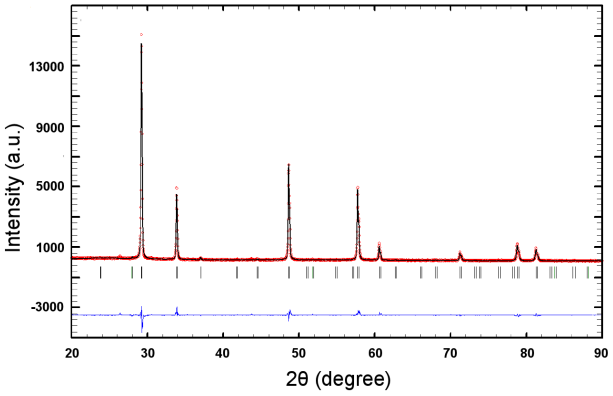

Figure 2. Results of the Rietveld refinement of the high-entropy ceramics obtained by pressureless sintering at 1650 °C for 4 h

pattern of the powder heat treated at 1500 °C (Fig. 1) shows that almost all resolved peaks correspond to the fundamental pyrochlore reflections representing an ordered pyrochlore structure in the space group 227.

The powder calcined at 1200 °C was subjected to the additional sintering process at 1650 °C to obtain dense ceramics. This powder was chosen for the final densification procedure since the XRD analyses show that during its calcination at 1200 °C a disorder-defective fluorite structure was obtained and the single phase was already formed. The Rietveld method was used to perform structural refinement of the obtained pyrochlore structure (Fig. 2). Pyrochlore phase has a space group 227 ($Fd\bar{3}m$) and accordingly it was adopted for the Rietveld structural refinement of the XRD pattern obtained for the sample sintered at 1650 °C. Since the most important structural parameters are the unit cell parameter and the positional $x(O_1)$ parameter they were selected for the refinement during the presented study. The positional $x(O_1)$ parameter represents the x coordinate of oxygen vacancy defect (O_1) and indicates the level of structural ordering, i.e. difference between the defective fluorite structure and the ordered pyrochlore structure. The x coordinate of O_1 can be in the range from 0.3125 (for ideal crystal structure) to 0.375 (for defective fluorite structure) [21]. In the present study, the x parameter of the obtained compositionally complex pyrochlore was determined to be 0.33873 indicating that the obtained densified ceramics depicts a highly ordered pyrochlore structure. The best fit between the calculated and observed XRD patterns of the sample sintered at 1650 °C is shown in Fig. 2, where all allowed Bragg reflections are shown by vertical bars. The unit cell parameter obtained by the Rietveld refinement is a = 10.5794(7) Å. The composition of the refined phase was set as $(La_{1/7}Sm_{1/7}Nd_{1/7}Pr_{1/7}Y_{1/7}Gd_{1/7}Yb_{1/7})_2(Sn_{1/3}Hf_{1/3}Zr_{1/3})_2O_7$.

The Raman spectrum of a pyrochlore structure is characterized by six Raman active modes according to the group theory, i.e. $\Gamma = A_{1g} + E_g + 4F_{2g}$. From the recorded Raman spectrum of the sintered ceramics, presented in Fig. 3, four out of six predicted Raman bands

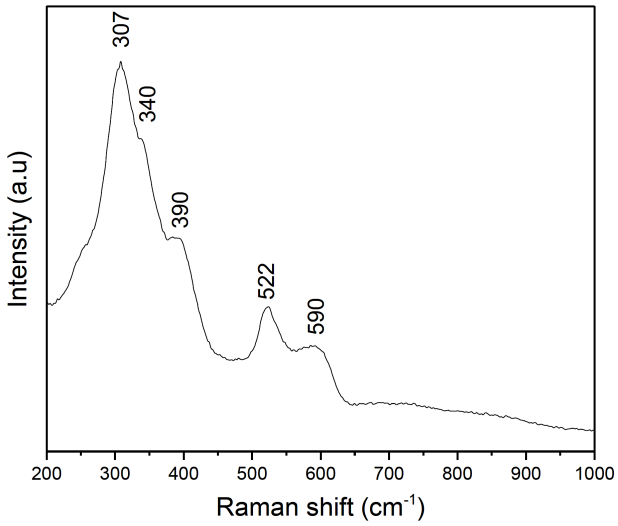

Figure 3. Raman spectrum of the sintered pyrochlore sample recorded in the range from 200 to 1000 cm^{-1}

for the high-entropy pyrochlore can be distinguished. The most intense Raman band observed at 307 cm^{-1} can be ascribed to the E_g mode due to the bending of the B-site elements with 6 oxygens, (Zr,Hf,Sn)O_6 [14]. The peaks observed at 389 and 589 cm^{-1} could be attributed to the T_{2g} modes, while the Raman band shown at 522 cm^{-1} can be identified as the A_{1g} mode. The remaining two bands that correspond to the T_{2g} modes and that should be present at approximately 470 and 845 cm^{-1} were not observed [25,26] probably due to the low intensity since the concentration of dopants is increased [27].

Microstructure of the sintered high-entropy ceramics is shown in Fig. 4. The obtained microstructure consists of densely compacted polyhedral grains with dimensions ranging from 0.5 to 5 μm. The attained density of the sintered high-entropy ceramic sample was 98 %TD, indicating a good sinterability of the starting oxides which acted as precursors. Moreover, the relatively easy densification process during the powder sintering at 1650 °C for 4 h was successfully achieved without the use of sintering additives. It can be noticed from Fig. 4 that all grains are in direct mutual contact without the presence of a secondary phase or an amorphous phase at the grain contact sites, as well as at the grain boundaries. Therefore, it can be assumed that the ceramic material with the observed microstructure will exhibit enhanced mechanical properties, especially at elevated temperatures. The achieved average microhardness value was 8.1 GPa, indicating the applicability of obtained high-entropy pyrochlore in industrial practice due to its good mechanical properties.

IV. Conclusions

The high-entropy multicomponent solid solution with nominal composition $(La_{1/7}Sm_{1/7}Nd_{1/7}Pr_{1/7}Y_{1/7}Gd_{1/7}Yb_{1/7})_2(Sn_{1/3}Hf_{1/3}Zr_{1/3})_2O_7$ was synthesized by classical solid state method. The pure oxides were precursors for the pyrochloric compound synthesis. Highly ordered crystalline high-entropy pyrochlore powder was obtained by heat treatment at 1500 °C. Sintering of the green compacts was undertaken without the use of sintering aids by applying the pressureless sintering process at 1650 °C for 4 h. Results of the Rietveld refinement confirmed that the positional parameter for x coordinate of O_1 has a value of 0.33873, which indicates that the obtained high-entropy ceramics shows a highly ordered pyrochlore structure. The resulting microstructure of the sintered high-entropy pyrochlore ceramics is characterized by a densely packed bimodal structure with polyhedral grains. The obtained grain size is in the range of 0.5 to 5 μm. The relative density of 98 %TD and hardness of 8.1 GPa were achieved.

Acknowledgments: This research was financially supported by the Ministry of Science, Technological Development and Innovation of the Republic of Serbia (Grant No. 451-03-47/2023-01/200017) and the Visiting Professor Program of the Chinese Academy of Sciences (2021VEA0003).

References

1. C. Oses, C. Toher, S. Curtarolo, "High-entropy ceramics", *Nat. Rev. Mater.*, **5** (2020) 295–309.
2. M.W. Glasscott, "Classifying and benchmarking high-entropy alloys and associated materials for electrocatalysis: A brief review of best practices", *Curr. Opinion Electrochem.*, **34** (2022) 100976

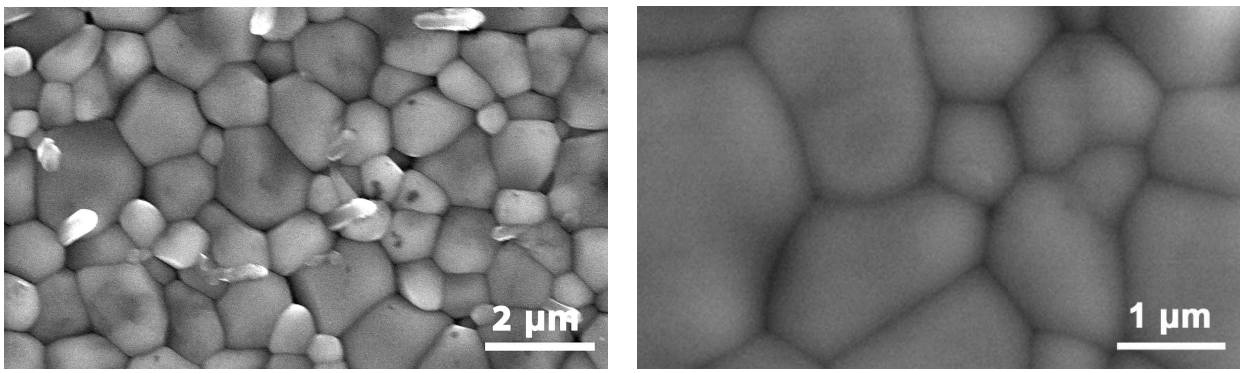

Figure 4. SEM micrographs of the high-entropy pyrochlore ceramics sintered at 1650 °C for 4 h

3. A. Sarkar, L. Velasco, D. Wang, Q. Wang, G. Talasila, L. de Biasi, C. Kubel, T. Brezesinski, S.S. Bhattacharya, H. Hahn, B. Breitung, "High entropy oxides for reversible energy storage", *Nat. Commun*., **9** (2018) 3400.
4. Y. Kong, G. Hu, K. Zhang, W.W. Hu, "Conductivity and electrochemical stability of Li^+ substituted high-entropy $Li_x(Mg_{0.2}Co_{0.2}Ni_{0.2}Cu_{0.2}Zn_{0.2})_{1-0.5x}O$ ceramics", *Process. Appl. Ceram.*, **16** (2022) 201–206.
5. M. Subramanian, G. Aravamudan, G.V. Subba Rao, "Oxide pyrochlores - A review", *Prog. Solid State Chem.*, **15** (1983) 55–143.
6. C.M. Rost, E. Sachet, T. Borman, A. Moballegh, E.C. Dickey, D. Hou, I.J. Jones, S. Curtarolo, J.P. Maria, "Entropy-stabilized oxides", *Nat. Commun.*, **6** (2015) 1–8.
7. H. Yamamura, H. Nishino, K. Kakinuma, K. Nomura, "Electrical conductivity anomaly around fluorite-pyrochlore phase boundary", *Solid State Ionics*., **158** (2003) 359–365.
8. J. Gardner, M. Gingras, J. Greedan, "Magnetic pyrochlore oxides", *Rev. Mod. Phys.,* **82** (2010) 53–107.
9. V. Risovany, A. Zakharov, E. Muravela, V. Kosenkov, R. Latypov, "Dysprosium hafnate as absorbing materials for control rods", *J. Nucl. Phys. Mater. Sci. Radiat. Appl.,* **335** (2006) 163–170.
10. R. Ewing, W. Weber, J. Lian, "Nuclear waste disposal – pyrochlore ($A_2B_2O_7$): Nuclear waste form for the immobilization of plutonium and minor actinides", *J. Appl. Phys.*, **95** (2004) 5071–5149.
11. X.Q. Cao, R. Vassen, D. Stoever, "Ceramic materials for barrier coatings", *J. Eur. Ceramic Soc.*, **24** (2004) 1–10.
12. A.S. Belousov, E.V. Suleimanov, D.G. Fukina, "Pyrochlore oxides as visible light-responsive photocatalysts", *New J. Chem.*, **48** (2021) 22531–22558.
13. S.K. Gupta, J.P. Zuniga, M. Abdou, M. Thomas, M. De Alwis Goonatilleke, B.S. Guiton, Y. Mao, "Lanthanide-doped lanthanum hafnate nanoparticles as multicolor phosphors for warm white lighting and scintillators", *Chem. Eng. J.*, **379** (2020) 122314.
14. B.P. Mandal, N. Garg, S.M. Sharma, A.K. Tyagi, "Preparation, XRD and Raman spectroscopic studies on new compounds $RE_2Hf_2O_7$ (RE = Dy, Ho, Er, Tm, Lu, Y): Pyrochlores or defect-fluorite?", *J. Solid State Chem.*, **179** (2006) 1990–1994.
15. Y. Mao, X. Guo, J.Y. Huang, K.L. Wang, J.P. Chang, "Luminescent nanocrystals with $A_2B_2O_7$ composition synthesized by a kinetically modified molten salt method", *J. Phys. Chem. C*, **113** (2009) 1204–1208.
16. D. Jin, X. Yu, H. Yang, H. Zhu, L. Wang, Y. Zheng, "Hydrothermal synthesis and luminescent properties of Yb^{3+} doped rare earth stannates", *J. Alloys Compd.*, **474** (2009) 557–560.
17. E. Pavitra, G. Seeta Rama Raju, J.S. Yu, "Solvothermal synthesis and luminescence properties of $Y_2Ti_2O_7$:Eu^{3+} spheres", *Phys. Status Solidi (RRL)*, **7** (2013) 224–227.
18. H. Kido, S. Komarneni, R. Roy, "Preparation of $La_2Zr_2O_7$ by sol-gel route", *J. Am. Ceram. Soc*., **74** (1991) 422–424.
19. N.A. Dhas, K.C. Patil, "Combustion synthesis and properties of fine-particle rare-earth metal zirconate $Ln_2Ze_2O_7$", *J. Mater. Chem.*, **3** (1993) 1289–1294.
20. B. Matovic, J. Maletaskic, J. Zagorac, V. Pavkov, R.S. Maki, K. Yoshida, T. Yano, "Synthesis and characterization of pyrochlore lanthanide (Pr, Sm) zirconate ceramics", *J. Eur. Ceram. Soc*., **40** (7) (2020) 2652–2657.
21. B. Matovic, D. Zagorac, I. Cvijovic-Alagic, J. Zagorac, S. Butulija, J. Ercic, O. Hanzel, R. Sedlak, M. Lisnichuk, P. Tatarko, "Fabrication and characterization of high entropy pyrochlore ceramics", *Bol. Soc. Esp. Ceram. Vidrio*, **62** [1] (2023) 66–76.
22. B. Matovic, J. Maletaskic, D. Bucevac, J. Zagorac, M. Fajar, "Synthesis, characterization and sintering of $Gd_2Hf_2O_7$ powders synthesized by solid state displacement reaction at low temperature", *Ceram. Int.*, **44** (2018) 16972–16976.
23. *PDXL Version 2.0.3.0 Integrated X-ray Powder Diffraction Software*. Tokyo (Japan): Rigaku Corporation, 2011: 196-8666.
24. A.F. Fuentes, S.M. Montemayor, M. Maczka, M. Lang, R.C. Ewing, U. Amador, "A critical review of existing criteria for the prediction of pyrochlore formation and stability", *Inorg. Chem.*, **57** (2018) 12093–12105.
25. C. Wang, Y. Wang, Y. Cheng, W. Huang, Z.S. Khan, X. Fan, Y. Wang, B. Zou, X. Cao, "Preparation and thermophysical properties of nano-sized $Ln_2Zr_2O_7$ (Ln = La, Nd, Sm, and Gd) ceramics with pyrochlore structure", *J. Mater. Sci.*, **47** (2012) 4392–4399.
26. B.E. Scheetz, W.B. White, "Characterization of anion disorder in zirconate $A_2B_2O_7$ compounds by Raman spectroscopy", *J. Am. Ceram Soc.*, **62** (1979) 468–470.
27. M. Glerup, O.F. Nielsen, F.W. Poulsen, "The structural transformation from the pyrochlore structure, $A_2B_2O_7$, to the fluorite structure, AO_2, studied by Raman spectroscopy and defect chemistry modeling", *J. Solid State Chem*., **160** (2001) 25.